

Enabling sub-THz Cloud RANs: Distributed Machine-Learning for Early HARQ Feedback Prediction

Barış Göktepe, Cornelius Hellge, Thomas Schierl and Slawomir Stanczak

Abstract

We propose novel HARQ prediction schemes for Cloud RANs (C-RANs) that use feedback over a rate-limited feedback channel (4 and 8 bits) from the Remote Radio Heads (RRHs) to predict at the User Equipment (UE) the decoding outcome at the BaseBand Unit (BBU) ahead of actual decoding. In particular, we propose a novel dual-input denoising autoencoder that is trained in a joint end-to-end fashion over the whole C-RAN setup. In realistic link-level simulations at 100 GHz in the sub-THz band, we show that a combination of the novel dual-input denoising autoencoder and state-of-the-art SNR-based HARQ feedback prediction achieves the overall best performance in all scenarios compared to other proposed and state-of-the-art single prediction schemes. At very low target error rates down to $1.6 \cdot 10^{-5}$, this combined approach reduces the number of required transmission rounds by up to 50% compared to always transmitting all redundancy.

I. INTRODUCTION

The need for more bandwidth and higher data rates drives the interest to new and even higher frequency bands. The 3rd Generation Partnership Project (3GPP) has responded to that need with a new work item targeting frequencies up to 71 GHz where large frequency bands are available. In particular, recent advances in hardware have paved the way for using these bands. Lately, these advances shift the focus of next generation mobile standards to even higher bands, i.e. the sub-THz and THz bands, which reach from 100 GHz up to 3 THz [1]. However, such

All authors are with Fraunhofer Heinrich Hertz Institute, 10587 Berlin, Germany (e-mail: first-name.lastname@hhi.fraunhofer.de)

This work has been submitted to the IEEE for possible publication. Copyright may be transferred without notice, after which this version may no longer be accessible.

high frequency bands, like the sub-THz and THz, come at the cost of highly depending on an unobstructed Line-Of-Sight (LOS) path, and significantly shorter channel coherence times, which require a higher control signaling overhead due to more frequent channel measurements [1]. Especially, the latter poses a bottleneck for the Channel State Information at the Transmitter (CSIT). CSIT, which requires extra delay [2], is essential to estimate the transmission parameters for a packet correctly. Due to the short coherence time, this delay makes the CSIT already obsolete when it is available at the transmitter. Although, exploiting geometrical properties of the environment and employing Machine Learning (ML) enables to predict the CSIT over larger time windows [2], the fast fading behavior of the channel may still make the channel estimation inaccurate. With high probability, an inaccurate CSIT results in an undecodable transmission, which can only be recovered using physical layer retransmission mechanisms, such as Hybrid Automatic Repeat reQuest (HARQ). However, HARQ, also known as reactive HARQ, increases the end-to-end latency because a feedback from the receiver is required at each retransmission round. This drawback is compensated by proactive HARQ that continuously transmits further retransmissions until an ACKnowledgment (ACK) is received [3], [4]. Proactive HARQ combines a high reliability with extremely short latencies [5]. Nevertheless, it trades these advantages for wasted spectral efficiency due to unnecessary retransmissions, which arrive during a successful decoding attempt [6].

Besides the shortened coherence time, the dependence on the LOS path also poses an issue for reliable communication, as any obstruction by an object on the LOS path causes a severe degradation of the channel. This lead the way to Cloud Radio Access Network (C-RAN) architectures where multiple reception points at different locations, i.e. Remote Radio Heads (RRHs), operate jointly to receive the packet. The Baseband Unit (BBU), which is responsible for higher layer processing, decodes the packet by combining all the individual received signals from the different RRHs. However, in the context of C-RAN architectures, the aforementioned drawbacks of reactive HARQ and proactive HARQ intensify even more due to the significantly larger feedback delay [7]. Hence, many papers in the scientific literature studied ways for reducing the feedback delay using prediction mechanisms. For architectures with a single reception point, different HARQ feedback prediction methods exist [6]–[19]. However, for architectures with multiple reception points, i.e. C-RANs, to the best of our knowledge only Khalili and Simeone proposed a Signal-to-Noise Ratio (SNR)-based HARQ prediction approach in [12]. Other prediction mechanisms, such as Log-Likelihood Ratio (LLR)-based and subcode-

based approaches, [6] and [14]–[19], have not been adapted yet for C-RAN architectures. Even for the SNR-based approach, no evaluation using realistic link-level simulations in the C-RAN context is available. Against this background, the contributions of this paper are summarized in the following:

- To tackle the HARQ prediction issue in C-RANs in a holistic manner, we present a novel Dual-Input Denoising Autoencoder (DIDA) that treats the subcode features at the individual RRHs as noisy versions of the joint ones is proposed. Furthermore, to reduce the dimensionality of the input features we propose over [19] and [6] a subcarrier-based averaging of the LLRs for the DIDA and LLR-based approaches.
- To enable state-of-the-art feedback prediction mechanisms for single reception points to be applied to C-RANs, we propose a distributed HARQ prediction setup with quantization of the feedback for over-the-air transmission and a combining rule at the User Equipment (UE). Within this setup, we develop a distributed Logistic Regression on LogLikelihood Ratios (LR-LLR) and Logistic Regression on Subcode features (LR-SC) based on [19].
- We simplify the SNR-based C-RAN HARQ prediction scheme proposed in [12], designated as Quantized Signal-to-Noise-Ratio (Q-SNR), and compare it to the other HARQ prediction approaches under realistic link-level simulations in the sub-THz band.
- Finally, we combine the DIDA and Q-SNR approaches creating a hybrid scheme and compare it to the other schemes within the context of the HARQ system evaluation methodology. We show that the combined approach achieves the overall best performance; in particular, reducing the average number of required Redundancy Versions (RVs) from 4.0 when always transmitting all RVs to 2.9 - 2.0.

A. Related work on HARQ feedback prediction

As mentioned in the previous section, different HARQ prediction schemes have been proposed and studied in the literature. This involves schemes from simple thresholding, e.g. [7], up to complex machine learning schemes, e.g. [16] and [19], which have gained interest in the past period, also in the context of the new Rel. 18 standardization [20]. In the following, we classify these schemes into three categories, where the second, LLR-based, and third, subcode-based, can also be interpreted as a joint single category, as they only differ in the processing but use the same raw data:

- 1) **Channel-estimation-based feedback prediction:** In [8], Makki et al. investigated a mixture of proactive and reactive HARQ protocols to reduce the expected latency. In the proposed scheme, the receiver accumulates the received signal until the accumulated sum channel gains, which are estimated over quantization regions, exceed a certain threshold associated with a sufficiently high decoding probability. In case of an unsuccessful prediction, i.e. the transmitted redundancy is not sufficient for successful decoding, the receiver switches to a reactive HARQ approach. In [7], Rost and Prasad and, in [12], Khalili and Simeone put the channel-estimation-based prediction schemes into the context of C-RANs and showed the benefits of early feedback in C-RANs with a non-ideal backhaul. Besides that, in [13], AlMarshed et al. proposed a Deep ML scheme that uses the received complex signal to estimate the decodability of a packet. Although being different from the previous schemes, we categorize this scheme as a channel-estimation-based approach because it does not involve the computation of LLRs or any other channel-code-aware features.
- 2) **LLR-based feedback prediction:** In [14] and [15], Berardinelli et al. used a Bit Error Rate (BER) estimate based on LLRs to predict the decoding outcome ahead of the actual decoding. They derived empirically a threshold on the BER estimate to predict the decodability. In contrast to the channel-estimation-based schemes, the LLRs contain inherently only a reduced form of the channel estimates. Nevertheless, different from the first category, the LLR-based schemes consider the whole received data signal for the prediction. The channel-estimation-based schemes rely only on pilot symbols, which are used to estimate the channel. As an improvement over the simple thresholding that was used by Berardinelli et al., Hummert et al. proposed in [16] to use a neural network that can mimic the decoder, designated as NN ForeCast. A hybrid pathway was proposed in [17] by AlMarshed et al., they combined both LLR- and channel-estimation-based features using a logistic regression. The proposed hybrid approach showed a significant enhancement over other approaches considering only one of both.
- 3) **Subcode-based feedback prediction:** In [6], [18] and [19], the authors proposed a feedback prediction mechanism that incorporates the partial decoding behavior of so-called subcodes. The subcodes reflect dependencies between received symbols arising from the structure of the channel code. This approach uses the LLRs as a basis, similar to the LLR-based feedback prediction; however, additional processing on the LLR based on the

knowledge of the code structure is applied to generate code-aware features. In particular, in [18], Göktepe et al. empirically determined thresholds for these code-aware features to predict the decoding outcome. As an improvement over this thresholding approach, in [19], the authors applied machine learning techniques, i.e. logistic regression, random forests, isolation forests and supervised autoencoders, on the LLR and code-aware features. Especially, the logistic regression and the supervised autoencoder have proven to be fruitful approaches to enhance the feedback prediction.

Apart from the previously described HARQ prediction schemes that are mainly designed for single reception points, [7] and [12] presented two similar approaches for implementing the channel-estimation-based feedback prediction in C-RANs. The works proposed collecting the channel gains and the SNRs over the received RVs, respectively. In [7], Rost and Prasad applied Gallager's error exponent to convert the channel estimation into an estimated error probability, as this metric is easier to work with:

$$\epsilon_i(R, \gamma) = c_1 e^{-NE_r(R, \gamma)}, \quad (1)$$

$$E_r(R, \gamma) = R_0(\gamma) - R, \quad (2)$$

where γ is the average SNR, R is the code rate, N is the code length, and R_0 is the cut-off rate associated with the SNR. See [21] for more details. After calculating Gallager's error exponent locally at the RRHs, they proposed applying a threshold to generate a positive or negative feedback. However, they ignored the case of multiple RRHs receiving the same packet. This was investigated by Khalili and Simeone in [12]. They proposed using a vector quantization as described in [22] to compress the channel state at the RRHs. Following the compression, the RRHs transmit this compressed feedback to the UE over a rate-limited feedback channel where a joint feedback is calculated. Furthermore, they also analyzed the impact of quantization of feedback on the system performance.

Notation: Throughout the paper, we use \mathbb{C} to denote the complex numbers and \mathbb{N} to denote the natural numbers. Furthermore, $\mathbb{C}^n, n \in \mathbb{N}$, denotes the n -dimensional complex vector space. $\mathbb{E}[\cdot]$ denotes the expected value and bold letters are used to indicate vectors, and bold and capital letters are used to indicate matrices. $diag(\cdot) : \mathbb{C}^n \rightarrow \mathbb{C}^{n \times n}, n \in \mathbb{N}$, denotes the mapping of an n -dimensional complex vector to an $n \times n$ complex diagonal matrix where the diagonal elements of the matrix are the components of the vector. Additionally, with some abuse of notation,

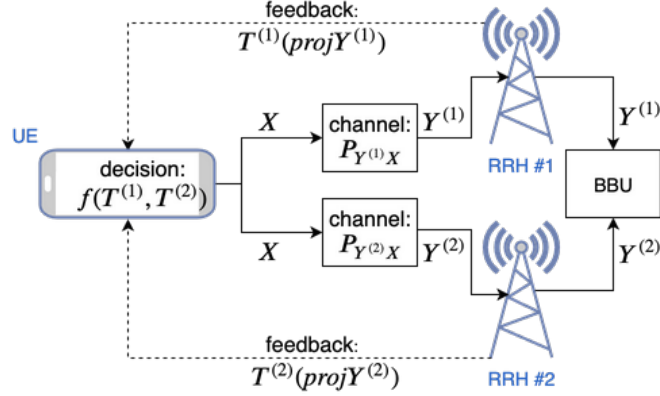


Fig. 1: Uplink C-RAN scenario with local HARQ feedback generated at the RRHs which is combined at the UE.

TABLE I: Definition of parameters

Parameter	Definition
n	Number of channel uses for the total transmission
p	Number of channel uses used at the time of prediction
$N_r^{(i)}$	Number of receive antennas at RRH i , $i = 1, 2$
b	Number of bits used for feedback from RRH to UE
T_{\max}	Maximum number of transmissions/RVs
M	Number of bits per channel use, i.e. QAM modulation order
N_{sc}	Number of subcarriers

$\text{proj}_p : \mathbb{C}^{k \times p} \times \mathbb{C}^{k \times (n-p)} \mapsto \mathbb{C}^{k \times p}$, $p, k, n \in \mathbb{N}$, $p < n$, denotes the projection which maps an element from the Cartesian product of two vector spaces on the first vector space. $\mathcal{N}(\mu, \sigma^2)$ designates the normal distribution with mean μ and variance σ^2 and $\mathcal{CN}(\mu, \sigma^2)$ designates its circularly-symmetric complex counterpart.

II. SYSTEM MODEL

Fig. 1 shows the system setup which is used throughout the paper. The definitions of commonly used variables are summarized in Tab. I. We assume an uplink scenario where a UE is transmitting a packet, which is received by two RRHs, over the air. For the links between the UE and RRH, we assume a single-input multiple-output (SIMO) setup with N_r receive antennas. After having received a packet at least partially, the RRHs generate a local feedback based on the different

prediction algorithms. The generated local feedback in turn is transmitted and combined at the UE. In the meanwhile, the received signals from the RRHs are accumulated and jointly decoded at the BBU which determines the final decoding outcome which is to be predicted by the proposed schemes.

Let $A := \mathbb{C}^n$ and $B := B_1 \times B_2 = \mathbb{C}^{N_r \times p} \times \mathbb{C}^{N_r \times (n-p)} = \mathbb{C}^{N_r \times n}$ designate the input and output sets. Furthermore, let the channels to each RRH be characterized by their respective joint probability measure $P_{Y^{(1)}X}$ and $P_{Y^{(2)}X}$. Given that n channel uses have been used, the channel probability measures represent the following association between the transmitted signal $\mathbf{x} \in A$ and the received signal vectors $\mathbf{Y}^{(1)}, \mathbf{Y}^{(2)} \in B$:

$$\mathbf{Y}^{(i)} = \mathbf{H}^{(i)} \text{diag}(\mathbf{x}) + \mathbf{Z}^{(i)}, \quad i = 1, 2, \quad (3)$$

where $\mathbf{H}^{(i)} \in B$, $i = 1, 2$, are the fading matrices and $\mathbf{Z}^{(i)} \in B$, $i = 1, 2$, are the noise vectors with each element distributed according to $\mathcal{CN}(0, 1)$. Further, we assume the fading matrices $\mathbf{H}^{(i)}$ to be consistent with the 3GPP Tapped Delay Line D (TDL-D) channel model, see [23] for more details.

To determine the final decoding outcome, the BBU combines and jointly decodes the received signal vectors $\mathbf{Y}^{(1)}$ and $\mathbf{Y}^{(2)}$ from the both RRHs. On the other hand, the RRHs calculate the feedback, which is a map $T^{(i)} : B_1 \rightarrow F$, $i = 1, 2$, where F is the sample space of the feedback. $T^{(i)}$ is specified differently depending on the prediction scheme. As we assume binary communication, the feedback sample space reduces to $F := \mathbb{F}_2^b$ where b is the number of bits used for the feedback transmission. Finally, to predict the decoding outcome at the BBU, the UE applies a combination rule $f : F \times F \rightarrow \{\text{ACK}, \text{NACK}\}$, which leads to corresponding UE behavior, i.e. stop transmitting or transmit more redundancy.

III. DISTRIBUTED EARLY HARQ STRATEGIES

In this paper, we consider early HARQ approaches that attempt to predict the decodability of a packet ahead of the actual decoding. In particular, we focus on early HARQ approaches that take only a part of the whole signal vector into account. In contrast to early HARQ approaches that use the whole signal vector, this approach ensures that the feedback can be provided at an earlier stage, which is crucial especially for latency constrained use cases. In the broadest sense, the prediction of decodability can be interpreted as statistical hypothesis testing, where the early HARQ predictor tries to discriminate between two probability distributions P and Q :

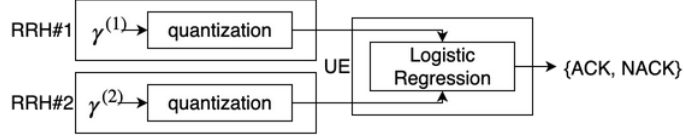


Fig. 2: SNR based distributed prediction approach.

the probability distribution of decodables P and the probability distribution of undecodables Q . Both distributions are determined by the channel probability distributions but also the behavior of the decoder at the BBU, hence also the properties of the code itself. This makes the exact characterization of P and Q extremely hard in practice and finding an optimal decision rule is a notoriously difficult problem.

In terms of the system model, the prediction is based p channel uses with $p < n$. Hence, in the context of Eq. (3), the received signals that are used for the prediction are described as follows:

$$\text{proj}_p \mathbf{Y}^{(i)} = \text{proj}_p \mathbf{H}^{(i)} \text{diag}(\text{proj}_p \mathbf{x}) + \text{proj}_p \mathbf{Z}^{(i)}, \quad i = 1, 2. \quad (4)$$

Hence, given $\text{proj}_p \mathbf{Y}^{(1)}$ and $\text{proj}_p \mathbf{Y}^{(2)}$, the binary hypothesis testing task is to decide between the two distributions

$$P := P_{D=\text{ACK}} | (T^{(1)}(\text{proj}_p \mathbf{Y}^{(1)}), T^{(2)}(\text{proj}_p \mathbf{Y}^{(2)})), \quad \text{and} \quad (5)$$

$$Q := P_{D=\text{NACK}} | (T^{(1)}(\text{proj}_p \mathbf{Y}^{(1)}), T^{(2)}(\text{proj}_p \mathbf{Y}^{(2)})), \quad (6)$$

where $D \in \{\text{ACK}, \text{NACK}\}$ represents the decoding outcome at the BBU with n channel uses available at the decoder.

A. Channel-estimation-based HARQ prediction (Q-SNR)

Channel estimation predictors focus on the estimated channel realization $\hat{\mathbf{H}}^{(i)}$, $i = 1, 2$, at each RRH. The estimation is performed based on known parts of the transmitted signal, e.g. reference signals such as Demodulation Reference Signal (DMRS). In the particular case of the paper's transmission model, one DMRS being used for the channel estimation is located at the beginning of each RV.

For channel-estimation-based prediction, we simplify the approach proposed in [12]. This simplified approach is referred to as Q-SNR. As depicted in Fig. 2, instead of using the Gaussian approximation for calculating the decoding probability, we propose a logistic regression with l_2

regularization, see [24] for more details, and balanced weight classes to learn the feedback combination rule f at the UE. The logistic regression approximates the decoding probability as $T^{(i)} := \frac{\exp(\beta_{10} + \beta_1^T v^{(i)})}{1 + \exp(\beta_{10} + \beta_1^T v^{(i)})}$ [25], where we determine the parameter set $\{\beta_{10}, \beta_1\}$ using the liblinear solver from the scikit-learn package [26]. We replace the vector quantization at the RRHs with the average received SNR γ_i , $i = 1, 2$ and apply a min-max normalization on γ_i following an equidistant quantization to b bits. This is motivated by Gallager's error exponent which depends on the average SNR, as seen in (1).

B. LLR based HARQ prediction (Q-LLR and LR-LLR)

The LLR based approaches assume that each element $x_i \in S \subset \mathbb{C}$, $i = 1, 2, \dots, n$, of the transmitted signal vector \mathbf{x} is i.i.d. and each element of the symbol set S representing M bits has the same probability. We are aware that this assumption does not hold in practice due to the channel code. Nevertheless, in the next section, we discuss a scheme that lacks this assumption. Using the i.i.d. assumption, the LLRs are calculated as

$$\Lambda_{i,j} := \log \frac{P(b_{i,j} = 1 | r_i)}{P(b_{i,j} = 0 | r_i)}, \quad (7)$$

where r_i , $i = 1, 2, \dots, n$, is the i -th received and equalized symbol and $b_{i,j}$, $j = 1, 2, \dots, M$, is the j -th bit in the i -th equalized symbol. This definition of LLRs leads to the following bit error probability:

$$v_l = \frac{1}{1 + e^{|\Lambda_{i(l),j(l)}|}}, \quad l = 1, 2, \dots, p, \quad (8)$$

where i and j map the index l to the corresponding symbol and the corresponding bit within the symbol, respectively. Against the background of [14], we provide in Eq. (8) a corrected version for the bit error probability [14, Eq. (7)]. The importance of this metric becomes clear under hard decision decoding for t -error correcting codes, as stated by the following theorem:

Theorem 1. *Let \mathcal{C} be an arbitrary t -error-correcting (n, k) -code on \mathbb{F}_2 under a corresponding hard-decision decoder, the code \mathcal{C} being transmitted over a memoryless channel and let $\Lambda \in \mathbb{R}^n$, be n log-likelihood ratios. Then $T : \mathbb{R}^n \rightarrow [0, 1]^n$ with $T(\Lambda) := \left(\frac{1}{1 + e^{|\Lambda_1|}}, \dots, \frac{1}{1 + e^{|\Lambda_n|}} \right)$ is a sufficient statistic to discriminate between decodable and undecodable receptions.*

Note that the calculation of LLRs assumes at least some knowledge about the channel. In particular, for an binary-input AWGN channel, correct LLR computation requires the knowledge of the SNR. The effect of defective channel estimation is neglected in this work. Furthermore, for

certain channels, which are discussed in more detail in the appendix, the Poisson approximation can be applied leading to an even stronger result:

Theorem 2. *Let \mathcal{C} be an arbitrary t -error-correcting (n, k) -code on \mathbb{F}_2 under a corresponding hard-decision decoder, the code \mathcal{C} being transmitted over a memoryless channel and let $\mathbf{\Lambda} \in \mathbb{R}^n$ be n log-likelihood ratios. Then, for a Poisson approximated channel*

- (i) $T : \mathbb{R}^n \rightarrow [0, 1]$ with $T(\mathbf{\Lambda}) := \frac{1}{n} \sum_{i=1}^n \frac{1}{1+e^{|\Lambda_i|}}$ is a sufficient statistic to discriminate between decodable and undecodable receptions of the code \mathcal{C} , and
- (ii) a uniformly most powerful (possibly randomized) test at α -level is given by

$$\Phi(T(\mathbf{\Lambda})) := \begin{cases} 1 & \text{if } T(\mathbf{\Lambda}) > C \\ \gamma & \text{if } T(\mathbf{\Lambda}) = C \\ 0 & \text{if } T(\mathbf{\Lambda}) < C \end{cases}, \quad (9)$$

with γ and C such that $\mathbb{E}_{U=t}[\Phi] = \alpha$.

This theorem shows that performing thresholding on the average bit error probability is optimal for t -error correcting codes under hard-decision decoding under certain channels. Modern channel codes, such as Low-Density Parity-Check (LDPC) codes, do not apply hard decision decoders, as this type of decoders is known to sacrifice a significant portion of the performance. Nevertheless, the stated theorems motivate the usage of this metric. The proofs of both theorems can be found in App. A. The scheme using the test in (21), where C is derived empirically and $\gamma := 0$, together with the quantization and combination rule as described in Sec. III-A, is called Quantized LogLikelihood Ratio (Q-LLR).

As n can be quite large and this hardens the training of the logistic regression, we propose a novel LLR averaging approach over the subcarriers, as depicted in Fig. 3. Over the duration of the coherence time of the channel, we assume an almost stable frequency selectivity. Hence, we can assume parallel AWGN channels for each subcarrier with either high or low SNR. As the Poisson approximation holds for high SNRs, as discussed in App. A, the averaging is a sufficient statistic according to Th. 2. However, this does not hold for the low SNR subcarriers. Nevertheless, assuming that these do not contribute much to the decodability, the information loss due to averaging can be neglected. This scheme with the previously described averaging is designated as LR-LLR. The averaged input features $\mathbf{v}^{(i)} := \{\bar{v}_1^{(i)}, \dots, \bar{v}_{N_{sc}}^{(i)}\}$, $i = 1, 2$ are fed into a logistic regression at each RRH, as shown in Fig. 4. These local logistic regressions are

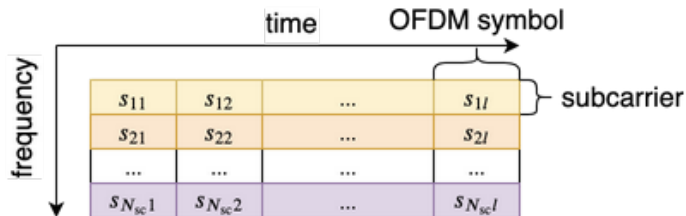


Fig. 3: LLR averaging over the duration of the transmission.

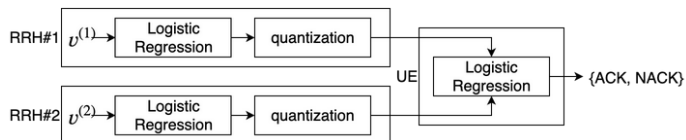


Fig. 4: LR based distributed prediction approach.

trained as the logistic regression in the UE in Sec. III-A using the BBU decoding outcome as target. For the quantization and the logistic regression at the UE, we use the same setup and parameters as for the Q-SNR in Sec. III-A.

C. Subcode-based HARQ prediction

Subcode-based HARQ predictors also take the LLRs as a basis. However, instead of assuming i.i.d. components of the signal vector X , the subcode-based prediction considers constraints defined by the parity-check matrix $\mathbf{P} \in \mathbb{F}_2^{L \times nM}$. The relation between the bit vector $\mathbf{b} := (b_{i,j}) \in \mathbb{F}_2^{nM}$, $i = 1, 2, \dots, n$, $j = 1, 2, \dots, M$, and the parity check matrix is defined as $\mathbf{P}\mathbf{b}^T = \mathbf{0}$. Message passing decoders, such as the min-sum implementation, iteratively update the LLRs based on \mathbf{P} , which is described by:

$$\Lambda_{i,j,k} = \Lambda_{i,j,k-1} + \sum_{m \in \mathcal{M}(i,j)} \beta_{m,k}, \quad (10)$$

where $\mathcal{M}(i,j)$ is the set of check nodes that are associated with the bit $b_{i,j}$ and $\beta_{m,k}^{(k)}$ is the check node to variable node message at the k -th iteration. In contrast to tree codes where message passing decoders always converge to the best solution, for modern LDPC codes the evolution of the LLRs can be interpreted as a sequence which may or may not converge to a "degraded" marginalization [27]. This behavior provides additional information on the healthiness of the received codeword.

1) *Logistic regression based subcode HARQ prediction (LR-SC)*: The scheme that is designated as LR-SC uses the averaged LLR feature and additionally the evolution of the averages over the iterations. On this vector of features, we apply the same processing, i.e. determination of T , quantization and combination rule, as shown in Fig. 4. Instead of the subcarrier-based LLR features, we input $N_{\text{It}} := 10$ averaged LLR evolution features $\mathbf{v} := (\bar{v}_k)$, $k = 1, 2, \dots, N_{\text{It}}$ with $\bar{v}_k = \frac{1}{N} \sum_{(i,j)} \frac{1}{1+e^{|\Lambda_{i,j,k}|}}$.

2) *Supervised dual-input denoising autoencoders (DIDA) for anomaly detection*: In the machine learning literature, autoencoders are well established for unsupervised anomaly detection tasks [28]–[30] due to their unprecedented dimensionality reduction capabilities [31]. Also for HARQ prediction purposes, a supervised autoencoder proposed in [19] outperformed other machine learning techniques, such as logistic regression, random forests, and others. However, the approach in [19] assumes a scenario with a single receive point. In this section, we extend this autoencoder to handle two separated RRHs. This novel approach, designated as DIDA, achieves a dimensionality reduction of the input features considering also joint features in the training phase. These joint features, which are generated at the BBU based on the combined signal, contain the most information on the decodability. Hence, we regard the subcode features of the RRHs as "noisy" versions of the joint features and apply a denoising autoencoder strategy. Denoising training is known to force the autoencoder to learn the actual structure of the data instead of simply learning the identity function, a known issue especially with overcomplete, high-capacity models [31]. Furthermore, we use two independent classifiers at each RRH to convert the reduced reconstruction features to a decodability feedback, which is afterwards combined at the UE classifier. We provide the details of the DIDA setup and training in App. B.

D. Data Transmission Model

In the high frequency spectrum, the coherence time of the channel is extremely small. Hence, the channel estimation based on that a resource allocation was assigned, may become already obsolete at the time of transmission. In our simulation setup, an RV spans over 28 Orthogonal Frequency Division Multiplexing (OFDM) symbols in time, which is equivalent to 31.25 μs . In contrast to that, the coherence time of the channel is approximated as [32, Eq. 9.1.27]:

$$T_0 \approx \frac{\lambda/2}{v}, \quad (11)$$

where λ is the wavelength and v is the traveling velocity. In our system model, the coherence time of the fading channel is comparable to the duration of an RV. This requires adaptive transmission

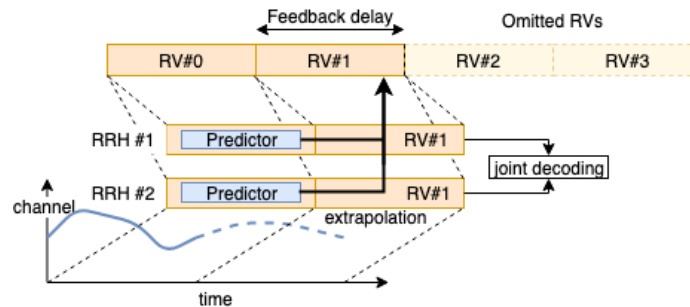


Fig. 5: Data transmission model incorporating the feedback delay.

schemes, such as proactive HARQ. Before starting a transmission, the UE determines a maximum number of RV transmissions depending on parameters, such as the latency budget or reliability requirement. After having determined the maximum number, the UE transmits the RVs in a consecutive manner, as depicted in Fig. 5. After receiving each RV, the RRHs provide feedback using the previously described prediction schemes. The UE decides based on a combination rule incorporating the feedback whether further RVs are required or not. This approach enables a good trade-off between reliability and spectral efficiency since some RVs are omitted. After having received all RVs from the UE, the RRHs forward the received signals to the BBU where a single decoding attempt is conducted. In this work, we simulate four RVs; hence, there are two prediction points:

- 1) the **first prediction point**, which uses the received RV#0 to decide whether RV#2 is required or not,
- 2) the **second prediction point**, which uses RV#0 and RV#1 to decide whether RV#3 is required or not.

E. Evaluation Methodology

In addition to achieving the reliability and the latency targets which are mandatory requirements, the performance of the HARQ schemes can be compared in terms of spectral efficiency. A higher spectral efficiency essentially results in an increased cell throughput. In contrast to commonly used classifier performance metrics, such as the precision and recall, the spectral efficiency provides a measure with direct takeover to practical scenarios. Especially, when considering edge cases with extremely low reliability requirements, metrics as the precision and recall may not provide a good metric for comparison [19].

Based on the renewal-reward theorem [33], the spectral efficiency is expressed as $\eta = \frac{\mathbb{E}[\mathcal{R}]}{N\mathbb{E}[T]}$, where $\mathbb{E}[\mathcal{R}]$ is an expected reward and $\mathbb{E}[T]$ is the expected number of requested transmissions and N is the number of channel uses per transmission. Furthermore, the reward is $\mathcal{R} := 0$ in case the transmission failed within the latency budget. In case the transmission was successful, \mathcal{R} is N_{packet} , the size of the packet in nats. Hence, the expected reward is given as $\mathbb{E}[\mathcal{R}] := (1 - \epsilon_{\text{tot}})N_{\text{packet}}$, where ϵ_{tot} is the associated total error probability.

The expected number of transmissions $\mathbb{E}[T]$ for a feedback delay of $\delta := 1$ is determined by the performance of the different estimators:

$$\begin{aligned} \mathbb{E}[T] &= 2((1 - \epsilon_1)(1 - \beta_1) + \epsilon_1\alpha_1) + T_{\max} \left(\prod_{j=1}^{T_{\max}-2} \epsilon_j(1 - \alpha_j) + (1 - \epsilon_j)\beta_j \right) \\ &+ \sum_{t=3}^{T_{\max}-1} t \left(\prod_{j=1}^{t-2} \epsilon_j(1 - \alpha_j) + (1 - \epsilon_j)\beta_j \right) (\epsilon_{t-1}(1 - \alpha_{t-1}) + (1 - \epsilon_{t-1})(1 - \beta_{t-1})), \quad (12) \end{aligned}$$

where M is the maximum number of transmissions, $\epsilon_i, i \in \{1, 2, \dots, T_{\max}-1\}$, are the error probabilities at the $(i+1)$ -th RV given that previous RVs were unsuccessful, $\alpha_i, i \in \{1, 2, \dots, T_{\max}-1\}$, are the false positive probabilities, i.e. predicting an unsuccessful decoding as an ACK, and $\beta_i, i \in \{1, 2, \dots, T_{\max}-1\}$, are the false negative probabilities, i.e. predicting an successful decoding as a NACK.

Also the total error performance ϵ_{tot} is determined by the error probabilities ϵ_i but also the false positive error probability α_i . The total error performance is given by [6]:

$$\epsilon_{\text{tot}} = \left(\sum_{t=1}^{T_{\max}-2} \left(\prod_{j=1}^{t-1} \epsilon_j(1 - \alpha_j) \right) \epsilon_t \alpha_t \right) + \left(\prod_{i=1}^{T_{\max}-2} \epsilon_i(1 - \alpha_i) \right) \epsilon_{T_{\max}-1}. \quad (13)$$

The false-positive probabilities and the false-negative probabilities behave in a conflicting manner, where the trade-off between both can be controlled by adjusting the bias s of the respective predictor. However, the functional relation between $\alpha_i(s)$ and $\beta_i(s)$ is not known. Hence, we determine 1000 admissible pairs $(\alpha_i(s_j), \beta_i(s_j)), j = 1, 2, \dots, 1000$, from the link-level simulations and interpolate them piece-wise linearly. Obviously, any false-positive false-negative curve of a reasonable predictor is a convex function, where at the extreme case when no prediction is possible, this function becomes a straight line connecting the points $(0, 1)$ and $(1, 0)$. Hence, a piece-wise linear interpolation is a conservative approximation, where the actual performance of the predictors at an interpolated point is expected to be better than the approximated value.

TABLE II: Link-level simulation assumptions for training, hyper and test set generation.

Transport Block (TB) size in bits (N_{Bits})	2000
RV duration (δ_t)	28 OFDM symbols
Transmission configuration	$T_{\text{max}} = 4$, $\delta_{\text{fb}} = 1$
Transmission bandwidth	100.0 MHz (16 PRBs)
Channel Code	Fifth Generation (5G) LDPC (see [35])
Modulation order and algorithm	4-QAM, Approximated LLR
Power allocation	Constant E_b/N_0
Number of antennas	$N_t = 1$, $N_r^{(1)} = 2$, $N_r^{(2)} = 2$
Waveform	3GPP OFDM, normal cyclic-prefix, 960 kHz subcarrier spacing
Channel type	1 Tx 2 Rx, TDL-D 30 ns, same SNR at RRHs 100 GHz, 120.0 km/h, ideal channel estimation
Equalizer	Frequency domain MMSE
Decoder type	Min-Sum (50 iterations)

With $\mathbf{s} := (s_1, s_2, \dots, s_{T_{\text{max}}-1})$ being the vector of biases per prediction, we derive the following optimization problem:

$$\begin{aligned} & \underset{\mathbf{s}}{\text{minimize}} && \mathbb{E}[T(\boldsymbol{\alpha}(\mathbf{s}), \boldsymbol{\beta}(\mathbf{s}))] \\ & \text{subject to} && \epsilon_{\text{tot}}(\boldsymbol{\alpha}(\mathbf{s})) \leq \epsilon_{\text{target}}, \end{aligned} \tag{14}$$

where ϵ_{target} corresponds to the overall reliability requirement. We use the Sequential Least Squares Programming (SLSQP) algorithm [34] with a Monte-Carlo approach to numerically find a valid solution to the aforementioned optimization problem.

F. Link-level simulation setup

To compare the performance of previously described HARQ prediction schemes, we conduct link-level simulations to collect the required LLR, subcode and channel estimation features. We choose the frame structure of the transmission, i.e. the mapping of the code block to resource elements and reference signals, e.g. DMRS, in accordance with the Rel. 16 3GPP specifications. Further, we use a subcarrier spacing of 960 kHz, which is currently being specified in the "NR operation up to 71 GHz" work item [36]. Tab. II summarizes the link-level parameters. We assume that different UEs are scheduled on different orthogonal time-frequency resources and hence, interference from other transmitters can be neglected. Furthermore, we assume a low correlation between the two receive antennas at each RRH, and no SNR difference between

TABLE III: Hyperparameters on which we conduct a grid search using a validation set.

Training, validation and test set sizes	3.5 M, 0.5 M, 1.0 M
Training epochs	100 - 400
Batch size	8192, 16392, 32784, 65568
Weighting factor λ	0.05, 0.1, 0.2, 0.3
Dropout probability	0.05, 0.1, 0.15, 0.2

the channels experienced at the two RRHs. For the decoding of the received signal vector, we apply an optimized min-sum algorithm [37] with 50 iterations. In contrast to that, the subcode prediction uses only 10 iterations. Hence, its complexity is only 1/5-th of the complexity of a full decoding attempt.

IV. SIMULATION RESULTS

In this section, we present the results for the different HARQ prediction approaches. For the DIDA prediction, Tab. III shows the hyperparameters on which we conduct a grid search using a validation set. We select the hyperparameters for each scenario based on the Area Under the false-positive-Curve (AUC) on the validation set. The corresponding test set is then used to determine the performance measures of the DIDA prediction. We also use the same validation and test approach to fit the logistic regressions, where we employ the training set to train the predictors locally at the RRHs and the validation set to train the quantization and joint combining rule at the UE.

In Tab. IV, we present the selected hyperparameters and the associated performance measures on the validation and test sets. Overall, we observe a good generalization behavior. The AUC on the validation and test sets lies in a similar range, where the AUC on the validation set is usually slightly underestimating the actual AUC on the test set, as expected. Only the AUCs at SNR 0 dB, prediction position 2 and at SNR -1 dB, prediction position 2 and feedback size of 4 bits show a significantly higher AUC on the test set compared to the validation set. Especially at 0 dB SNR, this can be explained by the extremely low Block Error Rates (BLERs) at which the code is operating at the second prediction position. Hence, the number of negative training samples (NACK) is much smaller compared to the lower SNR regimes.

A more interesting result is the behavior of the AUC performance on the test set over the feedback size. While at SNRs ≤ -2 dB a larger feedback size improves the prediction performance, we see

TABLE IV: AUC on validation and test sets.

SNR in dB	Pos.	(a) Feedback size 4 bits.			(b) Feedback size 8 bits.		
		Parameters 4 bits (epochs, batch, λ , dropout)	AUC on validation	AUC on test	Parameters 8 bits (epochs, batch, λ , dropout)	AUC on validation	AUC on test
-3	1	(200, 32784, 0.1, 0.15)	0.2387	0.2387	(200, 32784, 0.05, 0.1)	0.2376	0.2385
-3	2	(200, 8192, 0.05, 0.15)	0.0184	0.0284	(100, 65568, 0.1, 0.2)	0.0192	0.0235
-2	1	(200, 65568, 0.2, 0.2)	0.3240	0.3296	(400, 16392, 0.1, 0.05)	0.2519	0.2607
-2	2	(100, 32784, 0.05, 0.05)	0.0172	0.0370	(100, 65568, 0.2, 0.1)	0.0113	0.0191
-1	1	(100, 65568, 0.05, 0.2)	0.2417	0.2417	(400, 16392, 0.1, 0.05)	0.2519	0.2605
-1	2	(100, 16392, 0.1, 0.15)	0.0757	0.0667	(100, 65568, 0.05, 0.2)	0.0290	0.0285
0	1	(100, 16392, 0.2, 0.2)	0.2158	0.2077	(200, 32784, 0.05, 0.1)	0.2376	0.2385
0	2	(100, 32784, 0.2, 0.05)	0.0479	0.0898	(300, 16392, 0.2, 0.15)	0.0425	0.1044

the opposite behavior at the higher SNRs expect for -1 dB, prediction position 2. Intuitively, this behavior does not make sense as the 8 bit setup can simply emulate the 4 bit setup. However, due to the unbalanced training samples and the larger model capacity of the 8 bit setup, the training does not generalize as well as it does for the 4 bit setup.

A. False-positive and false-negative performance

The false-positive and false-negative mispredictions determine the performance of the predictor, as we can see from Eq. (12) and (13). Especially, the regime of low false-positives is of special interest because the cost of a false-positive misprediction is significantly higher than the cost of a false-negative misprediction. However, due to the finite size of the test sets, we have to deal with false-positives of zero, which makes a logarithmic scale unusable. Hence, a symmetrical logarithmic scale has been chosen for the false-positive axis. This scaling puts emphasis on the lower regime of the false-positive probabilities while keeping the zero point interpretable; however, special care has to be given to the linear scaling between the zero and the first step.

1) *4 bit feedback*: In Figs. 6, we show the false-positive misprediction probabilities over the false-negative rates of the different at different SNRs for the first prediction point. The Q-SNR clearly outperforms the other prediction times over the whole SNR range except for the 0 dB case, as we see in Fig. 6d. Here, DIDA outperforms Q-SNR at high false-negative probabilities > 0.7 . However, as the statistical accuracy in this range is limited, this result should not be

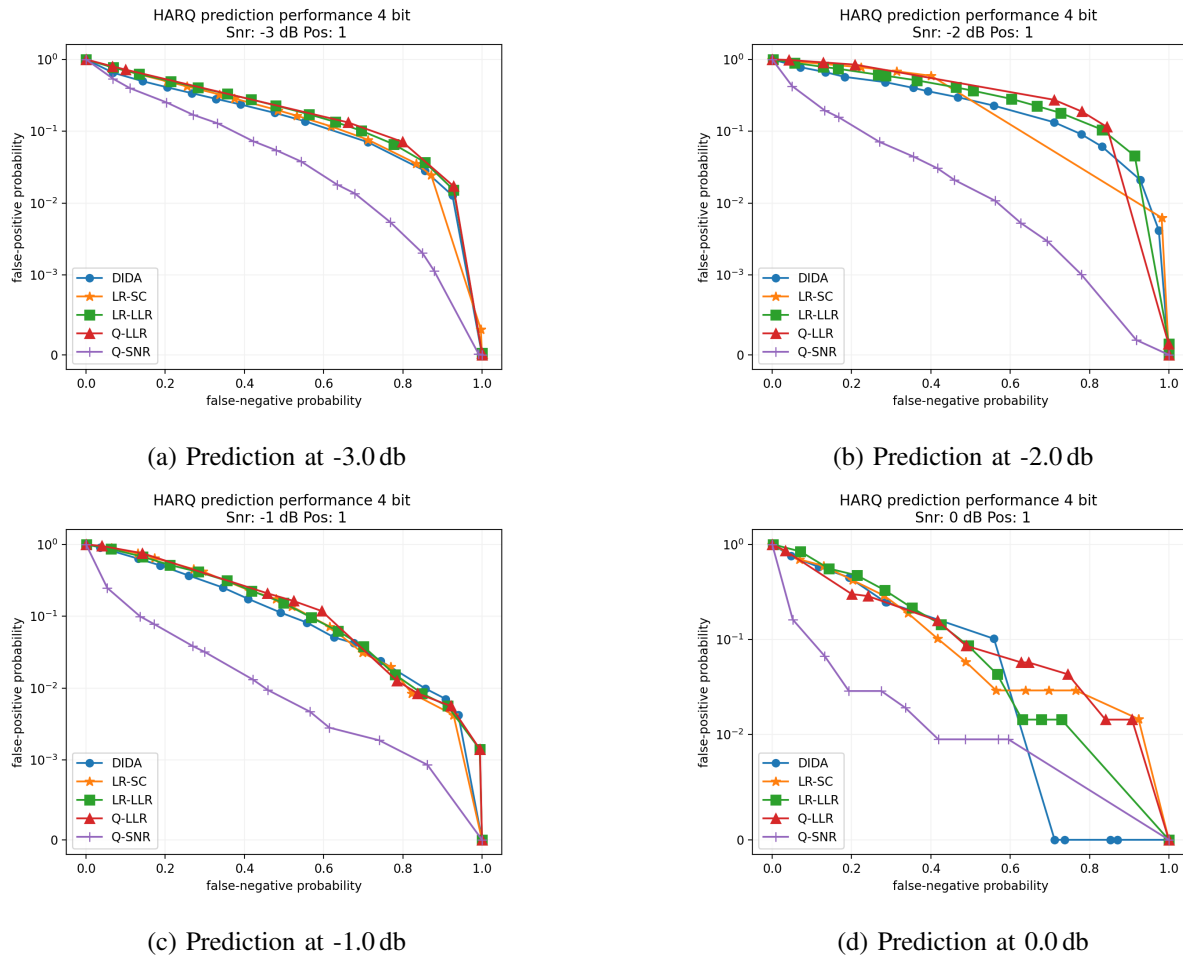


Fig. 6: False-positive prediction performance over false-negatives after the first RV for different SNRs with 4 bit feedback.

over-interpreted, especially considering that no false-positive events occurred at all within the test set for the DIDA in this range. Clearly, the Q-SNR approach dominates at the first prediction point with 4 bit feedback. Another interesting observation is that the accuracy of all schemes improves at higher SNRs. This can be seen from that at an SNR of -3 dB, the false-positive of 10^{-2} is reached at approximately 0.7 and 0.92 by the Q-SNR and the other schemes, respectively. The same false-positive is reached 0.6, 0.45 and 0.4 by the Q-SNR and 0.9, 0.8 and 0.62 at least for the case of DIDA at the higher SNRs of -2, -1 and 0 dB, respectively. Figs. 7 shows the false-positive probabilities over the false-negative probabilities at different SNRs for the second prediction point. Here, at the second prediction point, the situation is different from the first prediction point. Although Q-SNR performs quite well compared to LR-SC, LR-LLR and

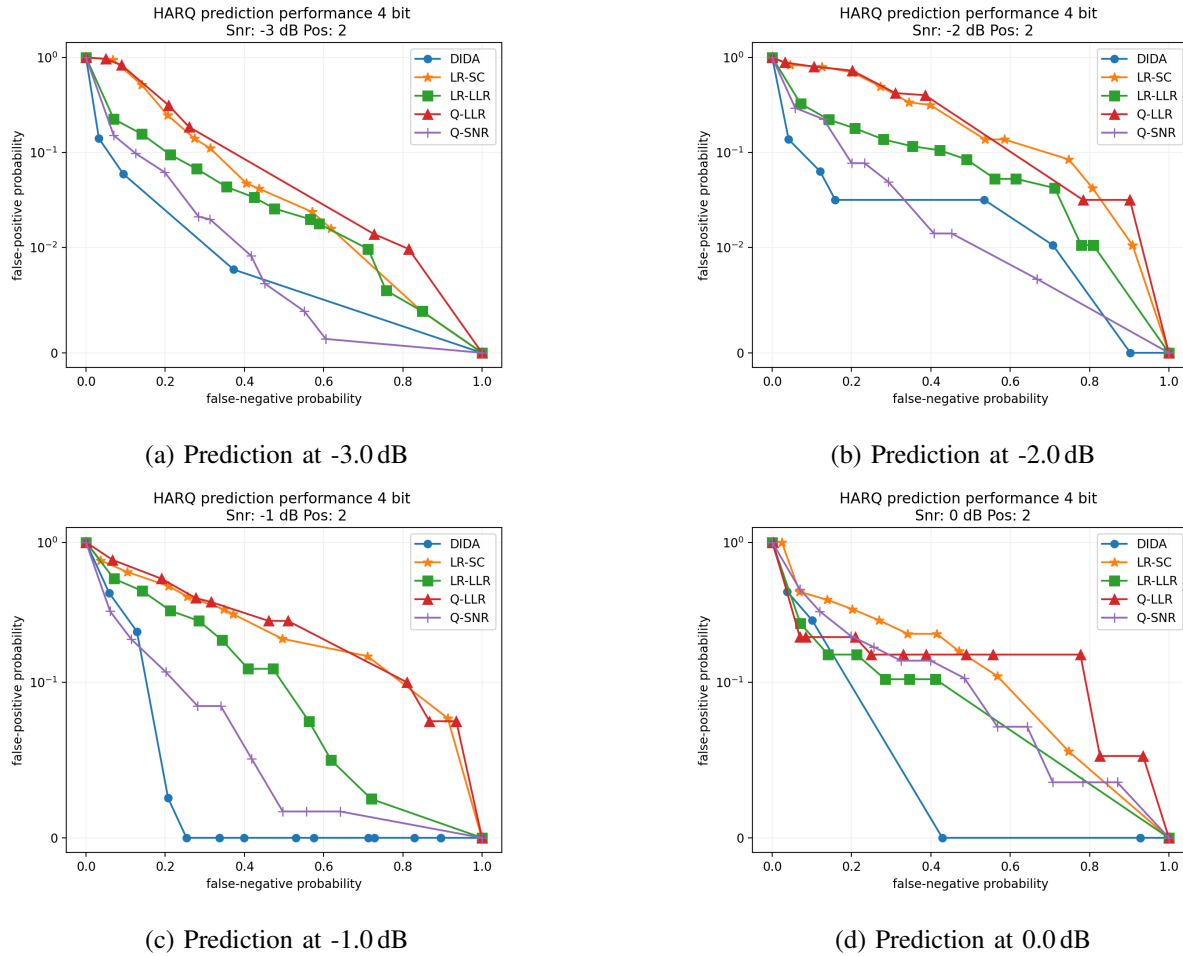


Fig. 7: False-positive prediction performance over false-negatives after the second RV for different SNRs with 4 bit feedback.

Q-LLR, DIDA achieves a better performance except for moderate false-negatives at an SNR of -2 dB, as shown in Fig. 7b. In particular at higher SNRs, it outperforms clearly all other schemes. Hence, in the case of 4 bit feedback, Q-SNR is a promising candidate predictor for the first prediction point and DIDA for the second prediction point. On the other hand, the ideal channel estimation clearly puts Q-SNR in advantage although a negative impact of realistic channel estimation may also be expected for the other schemes.

2) *8 bit feedback*: In Figs. 8, the false-positive probabilities is shown over the range of the false-negative probabilities for the first prediction point using the first RV only and predicting the decoding outcome of the first two RVs using 8 bit feedback. As it can be obviously noted, similar to the 4 bit feedback case, the false-positive performance of the different prediction schemes for

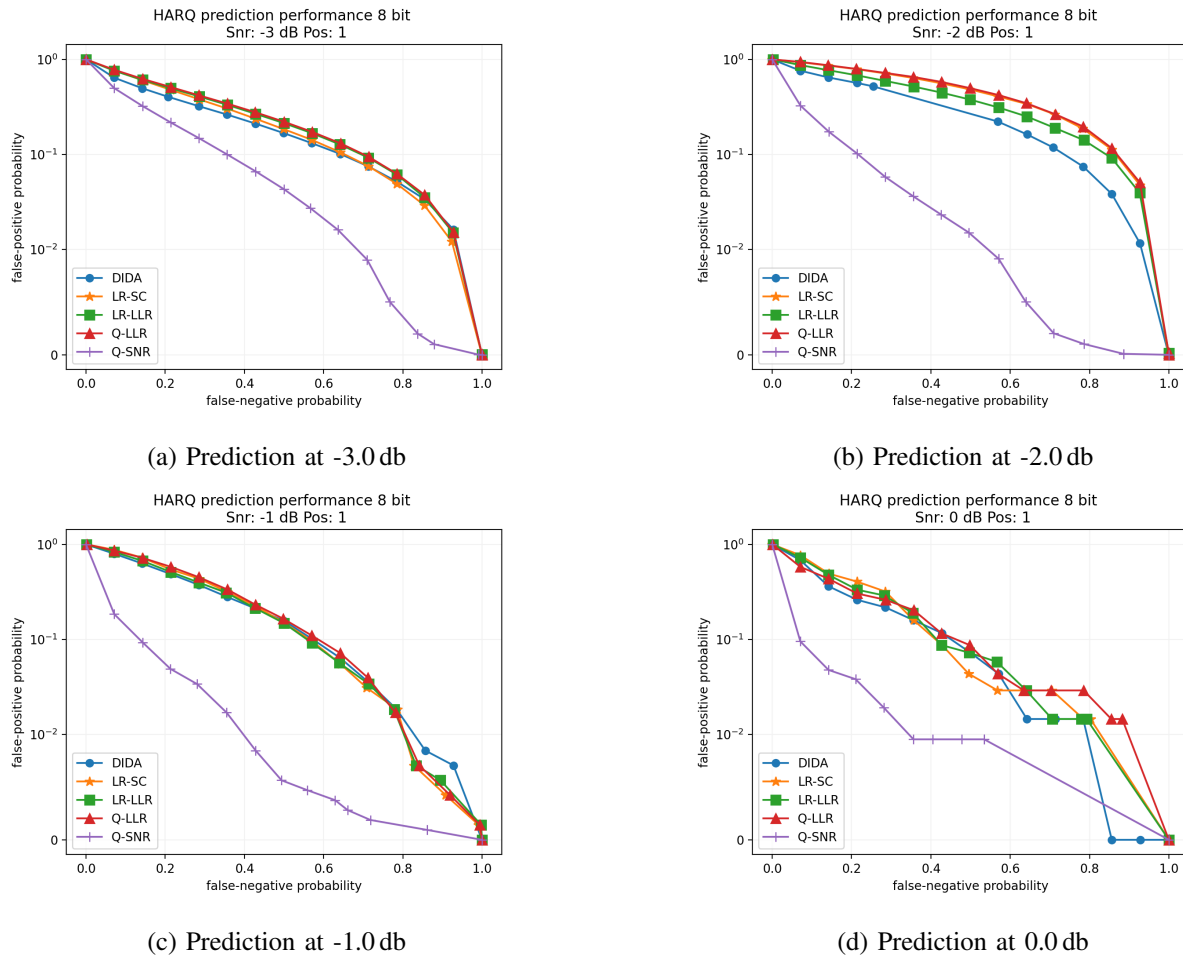


Fig. 8: False-positive prediction performance over false-negatives after the first RV for different SNRs with 8 bit feedback.

the LLR- and subcode-based schemes does not differ significantly. Only at an SNR of -2 dB and partly also at 0 dB, as depicted in Fig. 8b and 8d, respectively, DIDA achieves a slightly better performance than the LR-LLR, Q-LLR and LR-SC. However, as for the 4 bit feedback, Q-SNR achieves a significantly lower false-positive probability compared to all other schemes which is comparable to the performance with 4 bit feedback. Hence, for the first prediction point 4 bit feedback seems to be sufficient and allocating more bits for feedback does not significantly improve the performance. As for the 4 bit feedback case, an improved prediction accuracy is observed at higher SNRs. Fig. 9 shows the false-positive prediction performance over the false-negatives at the second prediction point using the first two RVs to predict the decoding outcome of the first three RVs. It can be seen that DIDA achieves the lowest false-positive

performance among all prediction schemes except for a few single points where Q-SNR reaches a slightly lower false-positive. Partly, this may also come from the ideal channel estimation and the performance with realistic channel estimation is to be researched. Compared to other LLR- and subcode-based schemes, DIDA clearly outperforms all schemes. Only Q-SNR achieves partly a comparable performance, in particular for the lowest SNR in Fig. 9a. At the second prediction point some performance differences for the 8 bit feedback compared to the 4 bit feedback are notable. To point out a few, DIDA reaches a false-positive of 10^{-2} at a false-negative of 0.7 at SNR -2 dB in Fig. 7b whereas with 8 bit feedback the same false-positive is reached at 0.2 in Fig. 9b. The same applies to the LR-LLR, which reaches $0.5 \cdot 10^{-1}$ at a false-negative of 0.5 at an SNR of 0 dB with 8 bit feedback in Fig. 9d, while in Fig. 7d the false-positive is still at 10^{-1} at the same false-negative. Also the Q-SNR achieves a false-positive of 10^{-2} at approximately 0.41 false-negative at an SNR of -3 dB in Fig. 7a. At the same false-negative, a false-positive of approximately $0.7 \cdot 10^{-2}$ is achieved with 8 bit feedback, as seen in Fig. 9a. Finally, the results show that increasing the capacity of the feedback channel also results in a slightly improved performance of the HARQ prediction at the UE.

B. HARQ system performance

In the previous section, we evaluated the false-positive and false-negative performance. However, the performance in a practical setup has to be shown to prove the efficiency of a scheme. Hence, we evaluate the different prediction schemes using the evaluation methodology described in Sec. III-E. Tab. V shows the expected number of transmissions that are required to obtain the mentioned target error rates at the given SNRs where the best performance among the LLR- and subcode-based approaches is highlighted using **bold** font and the overall best performance is furthermore underlined. We analyze the LLR- and subcode-based schemes separately from the Q-SNR scheme because the channel-estimation-based approach relies on a different data basis for the discrimination task. Then, with Q-SNR+DIDA we evaluate a joint combined approach. We join the advantages of both schemes by applying the Q-SNR for the first prediction point and the DIDA approach for the second prediction point.

As it can be noted, DIDA achieves the lowest expected number of transmissions at all SNRs for almost all target errors and SNR among the LLR and subcode based approaches. Only, for a few points other LLR- or subcode-based schemes achieve a better HARQ performance. Here, it has to be noted that these are all scenarios with higher target error rates with 0 dB and $1.6 \cdot 10^{-5}$

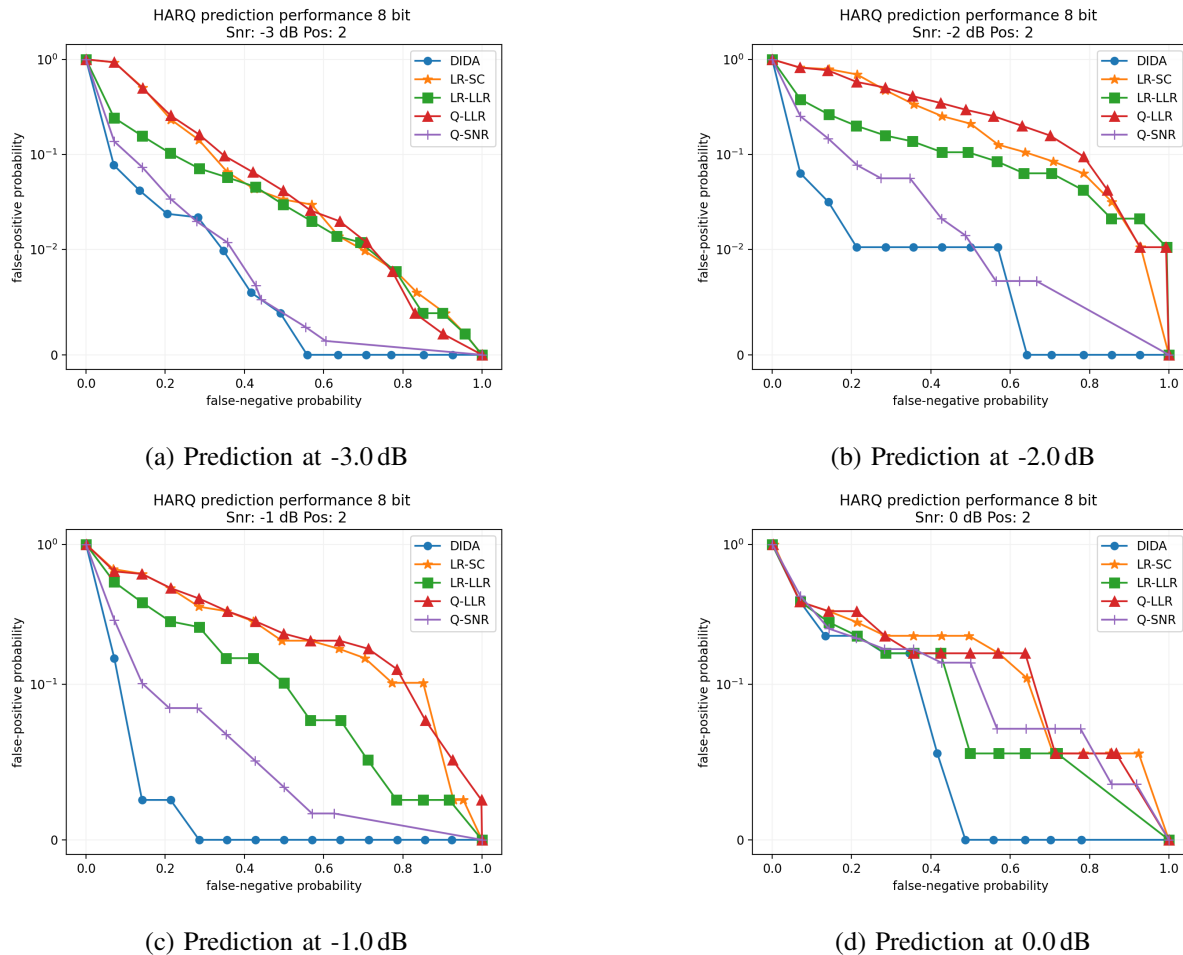


Fig. 9: False-positive prediction performance over false-negatives after the second RV for different SNRs with 8 bit feedback.

being the only exception. However, even for this exceptional result where LR-LLR achieves a better performance than DIDA, the performance of both schemes lies very close to each other. We explain this behavior by the results of the previous section where DIDA was by far the best predictor for the second prediction point however for the first prediction point the performance results did not differ significantly among the LLR- and subcode-based schemes. As we note from the values, the higher target error rates do not depend on the last, i.e. forth, RV. Hence, the superior performance of DIDA at the second prediction point does not play out, as the second prediction is responsible for requesting or omitting the forth RV. At lower target error rates this advantage plays out at its full extent.

Looking at HARQ performance results of the channel-estimation-based approach, i.e. Q-

TABLE V: HARQ system performance of the evaluated predictors with 4 bit and 8 bit feedback.

SNR	Target error	Feedback size	Q-LLR	LR-LLR	LR-SC	DIDA	Q-SNR	Q-SNR+DIDA
-3.0 dB	$8 \cdot 10^{-4}$	4	2.9777	2.9669	2.9604	2.9541	2.7434	<u>2.7220</u>
-3.0 dB	$8 \cdot 10^{-4}$	8	2.9684	2.9634	2.9613	2.9701	2.7203	<u>2.7002</u>
-3.0 dB	$2 \cdot 10^{-4}$	4	3.2885	3.1184	3.2554	3.0364	2.9805	<u>2.9093</u>
-3.0 dB	$2 \cdot 10^{-4}$	8	3.2717	3.1290	3.2617	3.0324	2.9547	<u>2.9007</u>
-2.0 dB	$5 \cdot 10^{-4}$	4	2.9102	2.8986	2.9252	2.8420	2.3080	<u>2.2961</u>
-2.0 dB	$5 \cdot 10^{-4}$	8	2.9175	2.9008	2.9152	2.8203	2.2883	<u>2.2807</u>
-2.0 dB	$8 \cdot 10^{-5}$	4	3.2721	3.0330	3.2547	3.0081	2.7269	<u>2.6582</u>
-2.0 dB	$8 \cdot 10^{-5}$	8	3.2785	3.0327	3.2659	2.9949	2.7200	<u>2.6627</u>
-1.0 dB	$8 \cdot 10^{-5}$	4	2.7007	2.6409	2.6355	2.5925	2.1883	<u>2.1704</u>
-1.0 dB	$8 \cdot 10^{-5}$	8	2.6557	2.6178	2.6178	2.6423	2.1743	<u>2.1577</u>
-1.0 dB	$3.5 \cdot 10^{-5}$	4	3.2764	3.1560	3.2180	3.0547	2.4666	<u>2.4163</u>
-1.0 dB	$3.5 \cdot 10^{-5}$	8	3.2223	3.1044	3.2071	3.0164	2.4067	<u>2.3629</u>
0.0 dB	$2 \cdot 10^{-5}$	4	2.7058	2.5991	2.5315	2.7423	2.0891	<u>2.0647</u>
0.0 dB	$2 \cdot 10^{-5}$	8	2.5702	2.5484	2.4889	2.5764	2.0546	<u>2.0405</u>
0.0 dB	$1.6 \cdot 10^{-5}$	4	3.2784	3.0052	3.3233	3.0733	2.1496	<u>2.1054</u>
0.0 dB	$1.6 \cdot 10^{-5}$	8	3.2784	3.0953	3.2515	2.9690	2.1014	<u>2.0773</u>

SNR, we see that the performance advantage of Q-SNR at the first prediction point trumps the advantage of the other schemes at the second prediction point in terms of the HARQ performance. Hence, it is not a surprise that the combined scheme Q-SNR+DIDA which combines both advantages achieves the best overall performance for all scenarios. As we see from Tab. V, Q-SNR+DIDA reduces the average number of transmitted RVs compared to always transmitting all RVs from 4 to approximately 2.91 with 4 bit feedback and 2.90 with 8 bit feedback at an SNR of -3 dB at $2 \cdot 10^{-4}$ target error rate. At the highest evaluated SNR, Q-SNR+DIDA brings this down to even 2.11 and 2.07 at 4 and 8 bit, respectively.

To gain more insights on where these efficiency gains come from, Tab VI shows the reduction of the transmission of RV#3 and RV#4 given that RV#3 was transmitted compared to always transmitting the respective RVs at the low target error rates, as these are the more interesting ones. Clearly, the LLR- and subcode-based schemes focus on reducing RV#4 to reach the required target error rates, as these are very low. Only at the highest SNR it can be observed that also RV#3 is significantly reduced by these schemes. This is consistent with the finding from the previous section that the performance of all schemes improves with increasing SNR and is also

TABLE VI: Usage reduction of RV#3 and RV#4 given that the previous RV was transmitted, of the evaluated predictors at low target error rates compared to always transmitting all RVs with 4 bit and 8 bit feedback.

SNR	Target error	Feedback size	Q-LLR	LR-LLR	LR-SC	DIDA	Q-SNR	Q-SNR+DIDA
			RV#3 in % RV#4 in %	RV#2 in % RV#3 in %	RV#2 in % RV#3 in %	RV#2 in % RV#3 in %	RV#2 in % RV#3 in %	RV#2 in % RV#3 in %
-3.0 dB	$2 \cdot 10^{-4}$	4	0.0 / -71.2	0.0 / -88.2	0.0 / 74.5	0.0 / -96.4	-9.0 / -92.3	-12.4 / -96.2
-3.0 dB	$2 \cdot 10^{-4}$	8	0.0 / -72.8	0.0 / -87.1	0.0 / -73.9	0.0 / -96.8	-11.6 / -92.1	-11.9 / -97.8
-2.0 dB	$8 \cdot 10^{-5}$	4	0.0 / -72.8	0.0 / -96.7	0.0 / -74.5	0.0 / -99.2	-30.8 / -95.0	-35.3 / -98.3
-2.0 dB	$8 \cdot 10^{-5}$	8	0.0 / -72.2	0.0 / -96.7	0.0 / -73.4	-1.6 / -98.9	-30.8 / -96.0	-35.3 / -97.6
-1.0 dB	$3.5 \cdot 10^{-5}$	4	0.0 / -72.4	0.0 / -84.4	0.0 / -78.2	-0.3 / -94.3	-57.4 / -90.5	-59.7 / -96.6
-1.0 dB	$3.5 \cdot 10^{-5}$	8	0.0 / -77.3	-1.2 / -88.6	0.0 / -79.1	-3.1 / -95.1	-64.3 / -86.0	-65.5 / -94.7
0.0 dB	$1.6 \cdot 10^{-5}$	4	0.0 / -72.2	-29.6 / -56.9	0.0 / -67.7	-12.9 / -76.7	-90.6 / -41.5	-90.6 / -88.3
0.0 dB	$1.6 \cdot 10^{-5}$	8	0.0 / -72.2	-22.0 / -59.6	-4.8 / -68.5	-36.2 / -48.0	-92.3 / -68.7	-92.3 / -99.8

notable for Q-SNR which in general reaches also a significant reduction for RV#3. As it can be noted, the combined scheme Q-SNR+DIDA achieves the best reduction of both RVs which is again consistent with previous findings. Especially, for the highest SNR, a reduction of up to -92.3% of RV#3 and -99.8% of RV#4 is achieved for a very low target error rate of $1.6 \cdot 10^{-5}$.

V. SUMMARY AND CONCLUSIONS

In this work, we proposed novel machine-learning assisted HARQ prediction schemes and evaluated them within the context of a C-RAN scenario in the sub-THz regime using link-level simulations. In particular, we extended the LLR- and subcode-based approaches proposed in [19] enabling their usage in a C-RAN setup by introducing a subcarrier-based averaging and adding quantization and a feedback combination module using a logistic regression. Furthermore, we propose a dual-input denoising autoencoder which is trained in an end-to-end fashion considering the full C-RAN setup including the quantization on the feedback channel. We compared these schemes to state-of-the-art C-RAN HARQ prediction mechanisms using the received SNR as a prediction basis with 4 and 8 bit feedback and furthermore, evaluated a combined approach making use of the advantage of both approaches. We showed that the dual-input denoising autoencoder achieves the best performance within the context of the HARQ evaluation methodology among the LLR- and subcode-based schemes. Furthermore, we found that at the first prediction,

the SNR-based prediction approach clearly outperforms all other schemes, however, not at the second prediction. Hence, we further showed that the combined scheme using the SNR-based and dual-input denoising autoencoder jointly achieves the overall best performance reducing the average number of requested RVs to 2.9 - 2.0 compared to 4 when always transmitting all RVs depending on the SNR and the rate of the feedback channel.

The results indicate that the combination of channel-estimation-based and subcode-based prediction mechanisms achieves the lowest mispredictions. In future research, it has to be studied whether a joint ML approach considering both feature types can exploit their diversity. Furthermore, the impact of non-ideal channel estimation on the performance of the different schemes has to be evaluated in further studies.

REFERENCES

- [1] T. S. Rappaport, Y. Xing, O. Kanhere, S. Ju, A. Madanayake, S. Mandal, A. Alkhateeb, and G. C. Trichopoulos, "Wireless communications and applications above 100 ghz: Opportunities and challenges for 6g and beyond," *IEEE Access*, vol. 7, pp. 78 729–78 757, 2019.
- [2] O. L. A. Lopez, N. H. Mahmood, H. Alves, C. M. Lima, and M. Latva-aho, "Ultra-low latency, low energy, and massiveness in the 6g era via efficient csit-limited scheme," *IEEE Communications Magazine*, vol. 58, no. 11, pp. 56–61, 2020.
- [3] N. H. Mahmood, R. Abreu, R. Böhnke, M. Schubert, G. Berardinelli, and T. H. Jacobsen, "Uplink grant-free access solutions for urllc services in 5g new radio," in *2019 16th International Symposium on Wireless Communication Systems (ISWCS)*, Aug. 2019, pp. 607–612.
- [4] T. Jacobsen, R. Abreu, G. Berardinelli, K. Pedersen, P. Mogensen, I. Z. Kovacs, and T. K. Madsen, "System level analysis of uplink grant-free transmission for urllc," in *2017 IEEE Globecom Workshops (GC Wkshps)*, Dec. 2017, pp. 1–6.
- [5] Y. Liu, Y. Deng, M. ElKashlan, A. Nallanathan, and G. Karagiannidis, "Analyzing grant-free access for urllc service," *IEEE Journal on Selected Areas in Communications*, vol. PP, Aug. 2020.
- [6] B. Göktepe, T. Rykova, T. Fehrenbach, T. Schierl, and C. Hellge, "Feedback prediction for proactive harq in the context of industrial internet of things," in *GLOBECOM 2020 - 2020 IEEE Global Communications Conference, 2020*, pp. 1–7.
- [7] P. Rost and A. Prasad, "Opportunistic hybrid arq—enabler of centralized-ran over nonideal backhaul," *IEEE Wireless Communications Letters*, vol. 3, no. 5, pp. 481–484, 2014.
- [8] B. Makki, T. Svensson, G. Caire, and M. Zorzi, "Fast harq over finite blocklength codes: A technique for low-latency reliable communication," *IEEE Transactions on Wireless Communications*, vol. 18, no. 1, pp. 194–209, 2019.
- [9] Z. Hou, C. She, Y. Li, L. Zhuo, and B. Vucetic, "Prediction and communication co-design for ultra-reliable and low-latency communications," *IEEE Transactions on Wireless Communications*, vol. 19, no. 2, pp. 1196–1209, 2020.
- [10] T. V. K. Chaitanya, "Harq systems: Resource allocation, feedback error protection, and bits-to-symbol mappings," Ph.D. dissertation, Linköping University Electronic Presss, Linköping, 2013.
- [11] J. Nadas, P. Klaine, L. Zhang, G. Zhao, M. Imran, and R. Souza, "Performance analysis of early-harq for finite block-length packet transmission," in *2019 IEEE International Conference on Industrial Cyber Physical Systems (ICPS)*, 2019, pp. 391–396.

- [12] S. Khalili and O. Simeone, "Uplink harq for cloud ran via separation of control and data planes," *IEEE Transactions on Vehicular Technology*, vol. 66, no. 5, pp. 4005–4016, 2017.
- [13] S. AlMarshed, D. Triantafyllopoulou, and K. Moessner, "Deep learning-based estimator for fast harq feedback in urllc," in *2021 IEEE 32nd Annual International Symposium on Personal, Indoor and Mobile Radio Communications (PIMRC)*, 2021, pp. 642–647.
- [14] G. Berardinelli, S. R. Khosravirad, K. I. Pedersen, F. Frederiksen, and P. Mogensen, "Enabling early harq feedback in 5g networks," in *83rd IEEE Vehicular Technology Conference (VTC Spring)*, May 2016, pp. 1–5.
- [15] G. Berardinelli, S. R. Khosravirad, K. I. Pedersen, F. Frederiksen, and P. Mogensen, "On the benefits of early harq feedback with non-ideal prediction in 5g networks," in *International Symposium on Wireless Communication Systems (ISWCS)*, Sep. 2016, pp. 11–15.
- [16] M. Hummert, D. Wübben, and A. Dekorsy, "Neural network-based forecasting of decodability for early arq," in *2021 17th International Symposium on Wireless Communication Systems (ISWCS)*, 2021, pp. 1–6.
- [17] S. AlMarshed, D. Triantafyllopoulou, and K. Moessner, "Supervised learning for enhanced early harq feedback prediction in urllc," in *2020 IEEE International Conference on Communication, Networks and Satellite (Comnetsat)*, 2020, pp. 26–31.
- [18] B. Göktepe, S. Fähse, L. Thiele, T. Schierl, and C. Hellge, "Subcode-based early harq for 5g," in *IEEE International Conference on Communications (ICC) Workshops*, May 2018.
- [19] N. Strodthoff, B. Göktepe, T. Schierl, C. Hellge, and W. Samek, "Enhanced machine learning techniques for early harq feedback prediction in 5g," *IEEE Journal on Selected Areas in Communications*, vol. 37, no. 11, pp. 2573–2587, 2019.
- [20] Qualcomm, "On ml over the nr air interface," RAN-Rel-18 workshop, TDoc RWS-210024, June 2021.
- [21] R. G. Gallager, *Information Theory and Reliable Communication*. USA: John Wiley & Sons, Inc., 1968.
- [22] D. Love, R. Heath, and T. Strohmer, "Grassmannian beamforming for multiple-input multiple-output wireless systems," *IEEE Transactions on Information Theory*, vol. 49, no. 10, pp. 2735–2747, 2003.
- [23] 3GPP, "Study on channel model for frequencies from 0.5 to 100 GHz," 3GPP, Tech. Rep. TR 38.901 v16.1.0, Jan. 2020.
- [24] "Scikit - linear models." [Online]. Available: https://scikit-learn.org/stable/modules/linear_model.html#logistic-regression
- [25] T. Hastie, R. Tibshirani, and J. Friedman, *The elements of statistical learning: data mining, inference and prediction*, 2nd ed. Springer, 2009. [Online]. Available: <http://www-stat.stanford.edu/~tibs/ElemStatLearn/>
- [26] F. Pedregosa, G. Varoquaux, A. Gramfort, V. Michel, B. Thirion, O. Grisel, M. Blondel, P. Prettenhofer, R. Weiss, V. Dubourg, J. Vanderplas, A. Passos, D. Cournapeau, M. Brucher, M. Perrot, and E. Duchesnay, "Scikit-learn: Machine learning in python," *Journal of Machine Learning Research*, vol. 12, pp. 2825–2830, 2011.
- [27] D. J. C. MacKay, *Information Theory, Inference & Learning Algorithms*. USA: Cambridge University Press, 2002.
- [28] Y. Zhou, X. Song, Y. Zhang, F. Liu, C. Zhu, and L. Liu, "Feature encoding with autoencoders for weakly-supervised anomaly detection," *IEEE transactions on neural networks and learning systems*, vol. PP, 2021.
- [29] B. Zong, Q. Song, M. R. Min, W. Cheng, C. Lumezanu, D. Cho, and H. Chen, "Deep autoencoding gaussian mixture model for unsupervised anomaly detection," in *International Conference on Learning Representations*, 2018. [Online]. Available: <https://openreview.net/forum?id=BJLHbb0->
- [30] H. Zenati, M. Romain, C.-S. Foo, B. Lecouat, and V. Chandrasekhar, "Adversarially learned anomaly detection," in *2018 IEEE International Conference on Data Mining (ICDM)*, 2018, pp. 727–736.
- [31] I. J. Goodfellow, Y. Bengio, and A. Courville, *Deep Learning*. Cambridge, MA, USA: MIT Press, 2016, <http://www.deeplearningbook.org>.
- [32] M. C. Jeruchim, P. Balaban, and K. S. Shanmugan, *Simulation of Communication Systems: Modeling, Methodology and Techniques*, 2nd ed. USA: Kluwer Academic Publishers, 2000.
- [33] S. Ross, *Stochastic processes*, ser. Wiley series in probability and statistics: Probability and statistics. Wiley, 1996.

- [34] “Scikit - slsqp.” [Online]. Available: <https://docs.scipy.org/doc/scipy-1.7.0/reference/optimize.minimize-slsqp.html>
- [35] MCC Support, “3GPP TS 38.212 v16.0.0,” 3GPP, Tech. Rep., Jan. 2020, pp. 19–30.
- [36] Qualcomm and Intel, “Revised wid: Extending current nr operation to 71 ghz,” 3GPP RAN#93 Electronic Meeting, TDoc RP-212637, Sep. 2021.
- [37] D. S. Shafiullah, M. R. Islam, M. M. A. Faisal, and I. Rahman, “Optimized min-sum decoding algorithm for low density pc codes,” in *2012 14th International Conference on Advanced Communication Technology (ICACT)*, 2012, pp. 475–480.
- [38] Y. Hong, “On computing the distribution function for the poisson binomial distribution,” *Comput. Stat. Data Anal.*, vol. 59, p. 41–51, mar 2013. [Online]. Available: <https://doi.org/10.1016/j.csda.2012.10.006>
- [39] T. Richardson and R. Urbanke, *Modern coding theory*. Cambridge University Press, 2008.
- [40] E. L. Lehmann, J. P. Romano, and G. Casella, *Testing statistical hypotheses*. Springer, 2005, vol. 3.
- [41] “Quantization.” [Online]. Available: <https://pytorch.org/docs/stable/quantization.html>
- [42] D. P. Kingma and J. Ba, “Adam: A method for stochastic optimization,” *CoRR*, vol. abs/1412.6980, 2014.

APPENDIX A

SUFFICIENT STATISTICS FOR HARD-DECISION DECODING

Algebraic block codes, such as Reed-Solomon codes, are usually decoded using hard-decision decoding. Hard-decision decoding involves quantizing the received signal to discrete values. Although the actual channel may be continuous, under the assumption that dependencies between the different symbols can be neglected, we can model the quantization and the physical channel as parallel discrete memoryless channels. In particular, for codes defined on the finite field \mathbb{F}_2 the discrete memoryless channels may be described by parallel binary symmetric channels, where the bit flip probabilities are given by the bit error probability $v_i = \frac{1}{1+e^{|\Lambda_i|}}$, $i = 1, 2, \dots, n$ with Λ_i being an LLR as defined in (7). For such a channel, any arbitrary codebook with d_{\min} being its minimum Hamming-distance and bounded minimum distance decoder pair results in a t -error-correcting code, where $t = \lfloor (d_{\min} - 1)/2 \rfloor$

Theorem 1. *Let \mathcal{C} be an arbitrary t -error-correcting (n, k) -code on \mathbb{F}_2 under a corresponding hard-decision decoder, the code \mathcal{C} being transmitted over a memoryless channel and let $\Lambda \in \mathbb{R}^n$, be n log-likelihood ratios. Then $T : \mathbb{R}^n \rightarrow [0, 1]^n$ with $T(\Lambda) := \left(\frac{1}{1+e^{|\Lambda_1|}}, \dots, \frac{1}{1+e^{|\Lambda_n|}} \right)$ is a sufficient statistic to discriminate between decodable and undecodable receptions.*

Proof. Let $\theta := \{1, 2, \dots, n\}$ be the parameter space and $U \in \theta$ a random variable representing the number of bit errors that have occurred. As the bit error probabilities are independent, the bit error probability given the received signal is $P_{\hat{X}_i \neq X_i | Y_i} = \frac{1}{1+e^{|\Lambda_i|}}$. Then, with Bayes’ theorem

$$p_{\Lambda|U=u}(\Lambda) = \frac{p_{\Lambda}(\Lambda)P_{U|\Lambda}(u)}{P_U(u)} = \frac{p_{\Lambda}(\Lambda) \sum_{A \in F_u} \prod_{i \in A} \frac{1}{1+e^{|\Lambda_i|}} \prod_{i \in A^c} \left(1 - \frac{1}{1+e^{|\Lambda_i|}}\right)}{P_U(u)}, \quad (15)$$

where p_{Λ} is the probability density of the LLRs and $P_{U|\Lambda}$ is the Poisson binomial probability mass function with $F_u = \{A \subseteq \theta : |A| = u\}$, defines a family of probability densities. Obviously, $p_{\Lambda|U=u}$ is a function of $T(\Lambda)$ and hence, T is a sufficient statistic by the factorization theorem. \square

The Poisson binomial distribution is usually hard to handle. However, for large n and small success probabilities¹ p_i , $i = 1, 2, \dots, n$, we can approximate it by a Poisson distribution [38] given by

$$P_{U|\Lambda}(u) \approx \frac{\left(\sum_i \frac{1}{1+e^{|\Lambda_i|}}\right)^u}{u!} \exp\left(\sum_i \frac{1}{1+e^{|\Lambda_i|}}\right). \quad (16)$$

The approximation error is bounded by [38]

$$\epsilon_{\text{approx}} := \sum_{u=1}^n \left| P_{U|\Lambda}(u) - \frac{\left(\sum_i \frac{1}{1+e^{|\Lambda_i|}}\right)^u}{u!} \exp\left(\sum_i \frac{1}{1+e^{|\Lambda_i|}}\right) \right| < 2 \sum_{j=1}^n \left(\frac{1}{1+e^{|\Lambda_j|}}\right)^2. \quad (17)$$

In particular, for a binary-input AWGN channel the LLRs are distributed according to $\Lambda_i \sim \mathcal{N}(\pm 2\frac{E_s}{\sigma^2}, 4\frac{E_s}{\sigma^2})$ [39]. Then, the probability of the LLRs taking large values increases with higher SNR. Let $\delta > 0$ be an arbitrary but fixed constant upper bound to the approximation error in (17) and a corresponding $C_\delta > 0$ such that $\delta = 2n \left(\frac{1}{1+e^{C_\delta}}\right)^2$. Then, for a binary-input AWGN channel the Poisson binomial distribution converges in probability to the Poisson approximation with increasing SNR:

$$\lim_{\frac{E_s}{\sigma^2} \rightarrow \infty} \mathbb{P}[\epsilon_{\text{approx}} < \delta] \geq \lim_{\frac{E_s}{\sigma^2} \rightarrow \infty} \left(\mathbb{P} \left[\mathcal{N}\left(\frac{2E_s}{\sigma^2}, \frac{4E_s}{\sigma^2}\right) > C_\delta \vee \mathcal{N}\left(\frac{2E_s}{\sigma^2}, \frac{4E_s}{\sigma^2}\right) < -C_\delta \right] \right)^n \quad (18)$$

$$\geq \lim_{\frac{E_s}{\sigma^2} \rightarrow \infty} \left(\mathbb{P} \left[\mathcal{N}\left(\frac{2E_s}{\sigma^2}, \frac{4E_s}{\sigma^2}\right) > C_\delta \right] \right)^n \quad (19)$$

$$= \lim_{\frac{E_s}{\sigma^2} \rightarrow \infty} \left(\mathbb{P} \left[\mathcal{N}(0, 1) > \frac{C_\delta - \frac{2E_s}{\sigma^2}}{2\sqrt{\frac{E_s}{\sigma^2}}} \right] \right)^n = 1, \forall \delta > 0. \quad (20)$$

Hence, in the high SNR regime the approximation provides a good estimate for the exact Poisson binomial distribution. In the following theorem, we designate such channels and their respective Poisson approximation as Poisson approximated channels. Under the Poisson approximation, the result from Th. 1 can be further tightened as stated by the following theorem:

¹Note that p_i are Poisson binomial success probabilities and not transmission success probabilities. In terms of transmission success, these are bit error probabilities.

Theorem 2. *Let \mathcal{C} be an arbitrary t -error-correcting (n, k) -code on \mathbb{F}_2 under a corresponding hard-decision decoder, the code \mathcal{C} being transmitted over a memoryless channel and let $\mathbf{\Lambda} \in \mathbb{R}^n$ be n log-likelihood ratios. Then, for a Poisson approximated channel*

- (i) $T : \mathbb{R}^n \rightarrow [0, 1]$ with $T(\mathbf{\Lambda}) := \frac{1}{n} \sum_{i=1}^n \frac{1}{1+e^{|\Lambda_i|}}$ is a sufficient statistic to discriminate between decodable and undecodable receptions of the code \mathcal{C} , and
- (ii) a uniformly most powerful (possibly randomized) test at α -level is given by

$$\Phi(T(\mathbf{\Lambda})) := \begin{cases} 1 & \text{if } T(\mathbf{\Lambda}) > C \\ \gamma & \text{if } T(\mathbf{\Lambda}) = C \\ 0 & \text{if } T(\mathbf{\Lambda}) < C \end{cases}, \quad (21)$$

with γ and C such that $\mathbb{E}_{U=t}[\Phi] = \alpha$.

Proof. (i) The first part is proved analogously to the first part of Th. 1, where $P_{U|\mathbf{\Lambda}}$ is replaced by the Poisson approximation as stated in (16).

(ii) Let $H : p_{\mathbf{\Lambda}|U \leq t}$ be a hypothesis and $K : p_{\mathbf{\Lambda}|U > t}$ be an alternative. The family of probability densities $\{p_{\mathbf{\Lambda}|U=k}\}_{k=1,2,\dots,n}$ possesses a monotone likelihood ratio with respect to the statistic $T(\mathbf{\Lambda})$:

$$\frac{p_{\mathbf{\Lambda}|U=k+1}(\mathbf{\Lambda})}{p_{\mathbf{\Lambda}|U=k}(\mathbf{\Lambda})} = \frac{P_U(k)}{P_U(k+1)} \frac{T(\mathbf{\Lambda})}{k+1}. \quad (22)$$

Hence, it fulfills the conditions of the fundamental lemma of Neyman and Pearson for monotone likelihood ratios [40, Th. 3.4.1]. \square

APPENDIX B

DUAL-INPUT DENOISING AUTOENCODER

In Fig. 10, we show the schematic design of the proposed DIDA. The network configuration for the encoders at each RRH of the denoising autoencoder is [FC($d,25$), FC($25,10$), FC($10,3$)] and for the decoder [FC($6,10$), FC($10,25$), Lin($25,d$)] where FC(x,y) \equiv [Lin(x,y), BN, ReLU, DO] and input dimension d . Furthermore, Lin(x,y) denotes a linear transformation layer, BN a Batch Normalization-layer, ReLU a ReLU activation layer and DO a dropout layer. As described earlier, we train the autoencoder like a denoising autoencoder where the input features at each encoder are the subcode features of the respective RRH $\mathbf{y}^{(i)}$, $i = 1, 2$, and the expected output features $\mathbf{y}^{(1+2)}$ are the subcode features from the combined evaluation at the BBU. This creates a link between the two RRHs via the BBU during the training phase, where the autoencoder

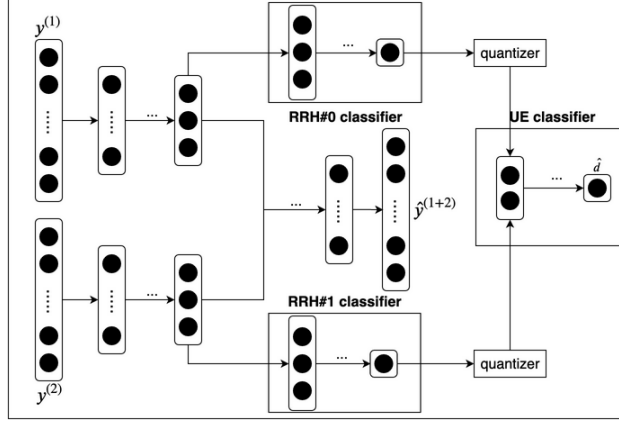


Fig. 10: A supervised dual-input denoising autoencoder (DIDA) to compress the feedback information at the RRHs and evaluate the combined result at the UE.

behaves like a denoising autoencoder with $\mathbf{y}^{(i)}$, $i = 1, 2$, each being a "noisy" version of $\mathbf{y}^{(1+2)}$. Obviously, for providing the feedback to the UE, the RRHs cannot use the joint subcode features $\mathbf{y}^{(1+2)}$. However, except for training the autoencoder the joint features $\mathbf{y}^{(1+2)}$ are not required. Hence, in practice each RRH computes its feedback locally although during training a link to the BBU is required.

Each RRH further contains a classifier that operates on the reduced form of the subcode features. The network configurations of the RRH classifiers each read as [FC(3,10), FC(10,5), Lin(5,2), SM] where SM is a softmax activation layer. Furthermore, we implement the quantization layer by a FakeQuantize layer in PyTorch using quantization-aware training [41]. Lastly, the network configuration of the UE classifier is given by [FC(2,10), FC(10,5), Lin(5,2), SM]. We train the DIDA in an end-to-end fashion using a loss function L that is composed by the L_2 norm and the cross-entropy between the predicted output \hat{d} and the actual decoding outcome d :

$$L((d, \mathbf{y}^{(1+2)}), (\hat{d}, \hat{\mathbf{y}}^{(1+2)})) = \frac{1}{N} \sum_{k=1}^N \|\mathbf{y}_k^{(1+2)} - \hat{\mathbf{y}}_k^{(1+2)}\|_2^2 + \lambda \left(d_k \log(\hat{d}_k) + (1 - d_k) \log(1 - \hat{d}_k) \right), \quad (23)$$

where N is the number of samples in a batch and λ is a fixed weight factor. The fixed weight factor is determined by conducting a hyperparameter optimization. To train DIDA under the given loss function, we use the Adam optimizer [42] at a learning rate of 0.001. Due to the nature of the sample data, the ratio between ACKs and NACKs is heavily imbalanced. Hence, we oversample the minority class, i.e. NACKs, to create a balance between ACKs and NACKs.